PROCEEDINGS of the
23rd International Congress on Acoustics

9 to 13 September 2019 in Aachen, Germany

# Vortex sound based calculations for the aeroacoustic noise of a centrifugal fan

Hakan DOGAN[1]; Martin OCHMANN[1]; Chris EISENMENGER[2]; Stefan FRANK[2]

[1] Beuth University of Applied Sciences Berlin, Germany

[2] HTW University of Applied Sciences Berlin, Germany

## ABSTRACT

Centrifugal fans are widely used in industrial applications such as home appliances, automobile industry and air-conditioning devices. In this work, we investigate the aerodynamic and aeroacoustic performance of a centrifugal fan with nine backward curved blades by means of computational fluid dynamics and aeroacoustics. In a few previous publications by the authors, some experimental and numerical results were presented and compared. Regarding the aeroacoustic computations, the far field noise was calculated by solving the Helmholtz equation using the boundary element method (BEM) or the finite element method (FEM). Moreover, FEM calculations using Lighthill's wave equation were also done. In the current paper, we perform vortex sound theory based aeroacoustic calculations, using Powell's analogy. The results obtained using vortex sound theory are compared with the theoretical/numerical approaches mentioned above, and with the experimental results. As stated by some previous researchers, although Lighthill's and Powell's formulations pose only slight differences mathematically, they exhibit considerably different numerical robustness. The application, numerical stability and accuracy of the two methods with regards to the current problem are investigated and compared.

Keywords: Vortex Sound, Centrifugal fan

## 1. INTRODUCTION

Centrifugal fans are used in many engineering applications such as engine turbocharger compressors [1], vacuum cleaners [2], refrigerators [3] and heat pump clothes-dryers [4]. Regarding the design of such fans, it is desired to increase the aerodynamic efficiency and to decrease the aeroacoustic noise. For the improvement of the aerodynamic performance, the number of blades and their skew-type, and the clearance between the fan and the volute of the housing have been adjusted in Ref. [5]. The following methods have been attempted in the literature for the noise reduction of centrifugal fans: the use of uneven blade spacing [6], resonators [7] or guide vanes [8], modifications to the tongue geometry and material (e.g. metal foams), and active noise cancellation.

Two of the fundamental aeroacoustic wave formulations are Lighthill's wave equation and Powell's wave equation. These two formulations are mathematically equivalent; Powell's formula [9] rewrites the right-hand side terms of Lighthill's equation in terms of the divergence of Lamb vector and Laplacian of the kinetic energy density. However, some researchers [10] have proposed that Powell's formulation is numerically more stable and accurate. In Ref. [11], we have investigated the aeroacoustic noise of a centrifugal fan using Lighthill's equation in integral form. In the current paper, we will present the numerical results based on the integral form of Powell's equation (the so-called vortex sound theory), and compare these two approaches in a low-Mach number problem.

The aerodynamic simulations for the centrifugal fan considered in this study were presented in Refs. [4, 12]. The Stress Blended Eddy model (SBES), as well as the Scale Adaptive Simulation and the Detached Eddy Simulation, were performed using ANSYS-CFX. The aerodynamic results from the SBES simulation for the reference fan will be used here for the aeroacoustic calculations. Moreover, the aerodynamic efficiency of the fan was experimentally tested according to the industrial norm DIN EN ISO 5801, which is compared in Ref. [4] with the numerical predictions for the efficiency.

[1] hdogan@beuth-hochschule.de, ochmann@beuth-hochschule.de
[2] c.eisenmenger@htw-berlin.de, stefan.frank@htw-berlin.de

## 2. FORMULATIONS

Powell's equation for aeroacoustic wave propagation is given as [9]

$$\frac{1}{c^2}\frac{\partial^2 p}{\partial t^2} - \nabla^2 p = \nabla \cdot (\rho\ \boldsymbol{\omega} \times \boldsymbol{v}) + \nabla^2 \frac{1}{2}\rho \boldsymbol{v}^2, \tag{1}$$

where $p$ is the acoustic pressure, $c$ is the sound speed, $\rho$ is the density, $\boldsymbol{\omega}$ is the vorticity vector, and $\boldsymbol{v}$ is the velocity vector. The first term on the right hand side is known as the Lamb vector (multiplied with density here for notational convenience):

$$\boldsymbol{L} = \rho\ \boldsymbol{\omega} \times \boldsymbol{v}. \tag{2}$$

Powell's equation (1) is mathematically equivalent to Lighthill's equation; the right hand is reformulated in terms of vorticity and velocity. In most flows (especially for the case of low Mach number as in the current study), the fluctuations of the last term are negligible because of the conservation of the kinetic energy. As such, one can write in frequency domain

$$\nabla^2 \hat{p} + k^2 \hat{p} = -\nabla \cdot \hat{\boldsymbol{L}}, \tag{3}$$

where $k$ is the wavenumber, $\hat{\boldsymbol{L}}$ is the Fourier transform of the Lamb vector, and $\hat{p}$ is the Fourier transform of pressure. Eq. (3) is the differential form of the inhomogeneous Helmholtz equation, it can be also represented in integral form. Accordingly, the acoustic pressure $\hat{p}(x_i)$ at an internal point $x_i$ within the domain can be obtained using the following integral equation [10]:

$$\hat{p}(x_i) = \int_{V_q} dV\ \ \hat{\boldsymbol{L}} \cdot \nabla G(x, y; k) + \int_{\Gamma} G \frac{\partial \hat{p}(x)}{\partial n} - \hat{p}(x) \frac{\partial G}{\partial n} d\Gamma, \tag{4}$$

where the Green's function $G$ is given by

$$G = \frac{e^{-ikr}}{4\pi r} \tag{5}$$

with $r$ being the distance between the collocation point $x_i$ and the integration points on the surface $\Gamma$ and in the volume $V_q$.

The governing equations given above can be solved in many ways; two of the most common methods are the Finite Element Method (FEM) and the Boundary Element Method (BEM). In this study, we use COMSOL FEM software to solve for the differential form (Eq. 3) and a modified version of the BEM code in Ref. [13] for solving the integral form (4).

For the CAA domain, we remove the rotationary domain in the CFD simulations and define a permeable interface ($\Gamma_{\mathrm{I}}$) outside the fan blades (see Fig. 1). The CFD pressure data at the virtual cylindrical interface outside the rotor is taken as the input.

Let $\Gamma$ denote the boundary enclosing the acoustic domain, e.g. $\Gamma = \Gamma_{\mathrm{I}} \cup \Gamma_{\mathrm{w}} \cup \Gamma_{\mathrm{o}}$, where $\Gamma_{\mathrm{I}}$ is the permeable surface (the inlet), $\Gamma_{\mathrm{o}}$ is the circular outlet of the duct, and $\Gamma_{\mathrm{w}}$ are the rigid side walls between the inlet and outlet (Fig. 1). At the permeable interface $\Gamma_{\mathrm{I}}$, the acoustic pressure is prescribed by taking the Fourier transform of the time-domain pressure values ($p_{\mathrm{I}}$) obtained in the CFD simulations:

$$\hat{p}(\boldsymbol{x}, f) = \hat{p}_{\mathrm{I}}(\boldsymbol{x}, f) \qquad \boldsymbol{x} \in \Gamma_{\mathrm{I}}. \tag{6}$$

On the rigid side walls, the particle velocity is zero. Therefore, the hard-wall condition is employed, i.e.

$$\frac{\partial \hat{p}(\boldsymbol{x})}{\partial n} = 0 \qquad \boldsymbol{x} \in \Gamma_{\mathrm{w}}. \tag{7}$$

At the outlet, the plane-wave impedance condition is prescribed:

$$Z(\boldsymbol{x}) = \rho c \qquad \boldsymbol{x} \in \Gamma_{\mathrm{o}}. \tag{8}$$

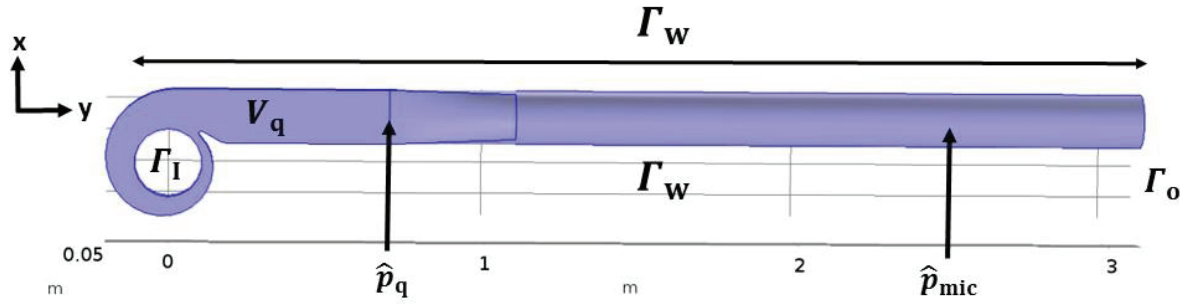


Figure 1 – Acoustic calculation domain with the cylindrical interface outside the rotor domain

The domain for the quadrupole sources is the volume $V_q$ between the cylindrical interface and $y$=0.7 m plane. For the simulations using the integral form, we calculate the acoustic pressure $\hat{p}_q$ in the midpoint of $y$=0.7 m plane, because the effects of turbulent sources in a point inside the domain are of interest. In the region $y$>0.7 m, the acoustic waves propagate as plane waves below the cut-off frequency [13]. Therefore, the acoustic pressure $\hat{p}_{mic}$ at the location of the microphones can be calculated analytically as

$$\hat{p}_{mic} = \hat{p}_q \; e^{-ik(y_m - y_I)}, \tag{9}$$

where $y_m = 2.47$ m is the $y$-coordinate of the microphones, and $y_I$ is the $y$-coordinate of the end of near field (CFD) domain, e.g. $y_I = 0.7$ m.

## 3. EXPERIMENTAL SETUP

The acoustic noise measurements were carried out according to the international norm ISO 5136 using the in-duct method. The test facility (in Fig. 2) was installed inside a semi-anechoic room. An anechoic termination was mounted to the outlet (at $y$=3.1 m). Three high precision slit-tube microphones were installed inside the duct on $x$-$z$ plane, at $y$=2.47m.

The noise recordings were done with a duration of 35 seconds and were repeated ten times in order to reduce the standard deviation error of the results. The Fourier transform of the time signals were computed with the software Samurai from Sinus Acoustics, and the obtained sound pressure levels (SPLs) were averaged over ten samples. The final displayed results for the noise levels require some corrections because of the mean flow velocity and the shield protection of the slit microphones. The experimental noise spectra for different frequency resolutions are given in Fig. 3.

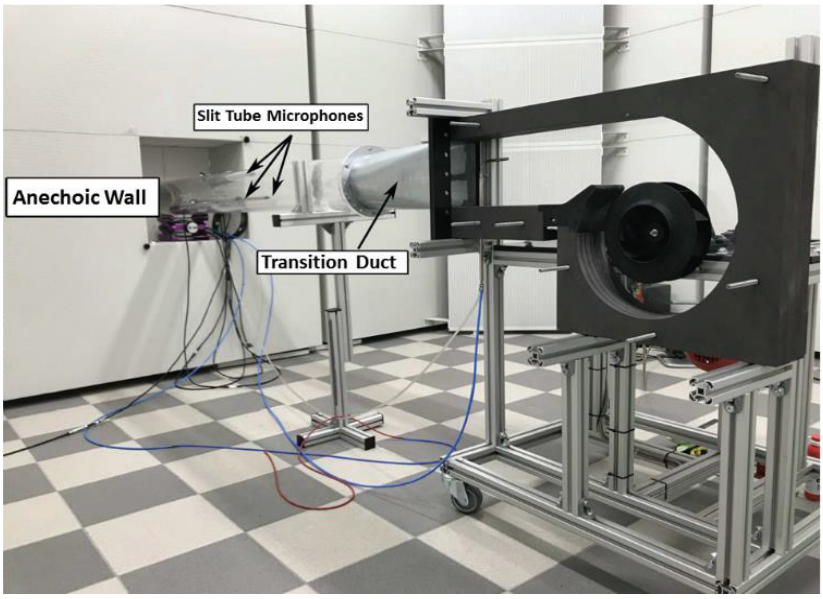


Figure 2 – The experiment setup in the semi anechoic room at HTW Berlin

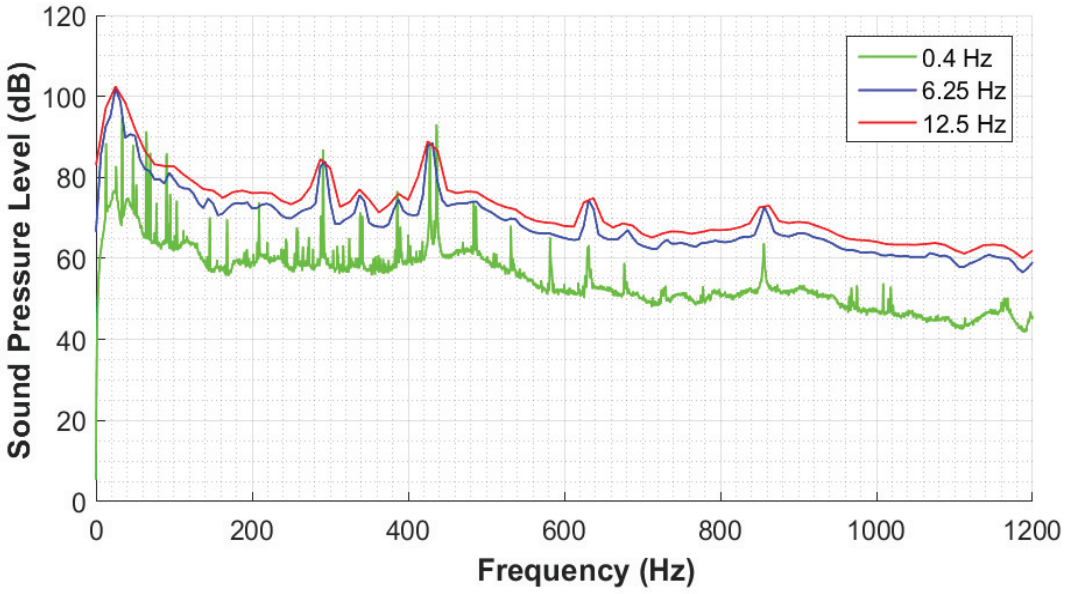


Figure 3 – The experimental noise spectra at different frequency resolutions (0.4 Hz, 6.25 Hz and 12.5 Hz)

## 4. RESULTS

### 4.1 Components of Lamb vector

In order to give a qualitative image of the Lamb vector, the *x* and *y* components are plotted in Fig. 4 using an interpolation function in the Finite Element software COMSOL. Figure 4(a) and 4(b) show the distribution of the x and y components, respectively, in frequency domain at the blade passing frequency (BPF) 429 Hz. It is observed that the magnitude of Lamb vector is the highest near the rotor domain where turbulent fluctuations are the largest. Towards the outlet of the duct, the magnitude of Lamb vector decreases at least one order.

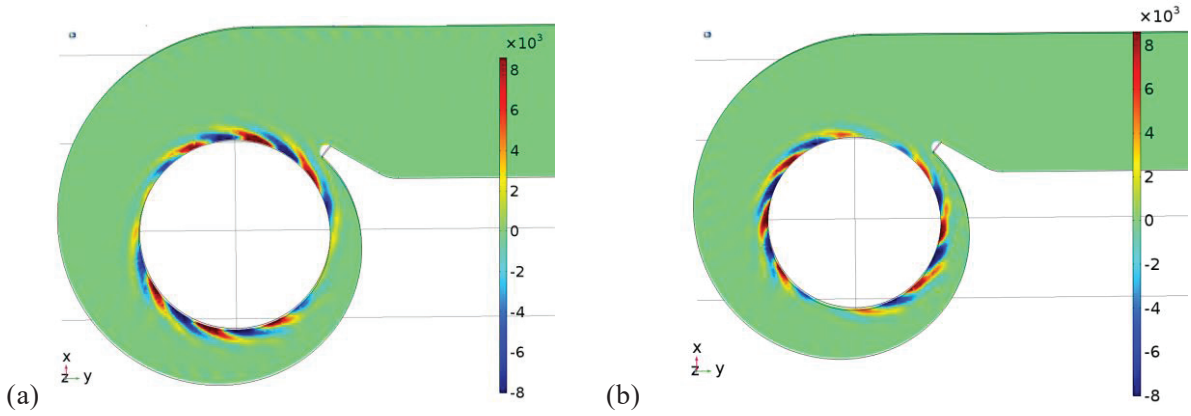


Figure 4 – The *x*- and *y*-components of Lamb vector at 429 Hz, plotted using COMSOL FEM software

### 4.2 Sound pressure level (SPL)

The results of the frequency-domain simulations will be shown hereafter. All of the numerical simulations here have a frequency resolution of ~11.95 Hz. Hence, the results are compared to the experimental spectrum with 12.5 Hz resolution, where applicable. The strongest component in the noise spectra is obtained at the BPF. In Fig. 5, the distribution of the SPL at the BPF is shown, where the COMSOL FEM is used based on the differential equation (3). The components of the Lamb vector have been imported into the program, using the 'Dipole Domain Source' feature available in the

Frequency Domain Pressure Acoustics module. In the region $y \approx 0.5$ m to the outlet of the duct, a constant SPL of ~93 dB is obtained.

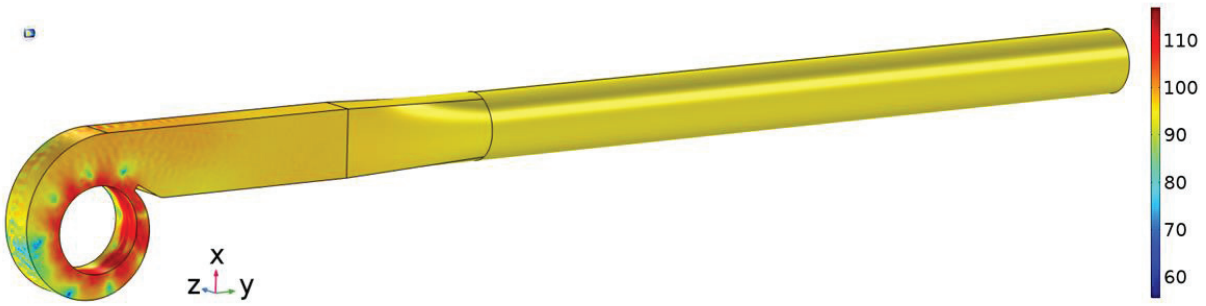


Figure 5 – The sound pressure level SPL (decibel) in the domain at 429 Hz computed with COMSOL FEM

The sound pressure level results over the whole frequency range are shown in Fig. 6. The results in Fig. 6 are obtained based on the integral formulation (4) solved with BEM. The black line in the figure shows the results with the volume integral in (4), e.g. including the effects of the turbulent noise contribution. The blue line presents the results for the surface integral terms in Eq. (4), which is the Kirchhoff-Helmholtz integral equation. It is seen that the effects of quadrupole sources on the total sound pressure level are more pronunced in the low frequency range.

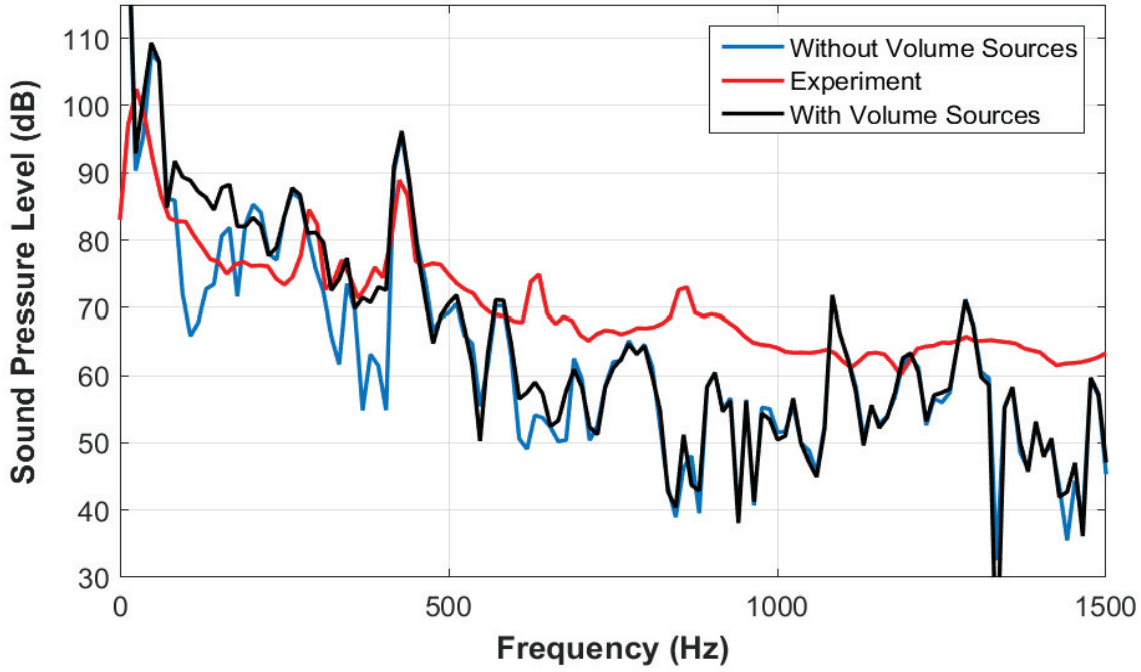


Figure 6 – The SPL with/out volume sources (the integral with Lamb vector) computed with BEM

### 4.3 Comparison of Powell's and Lighthill's formulations

The comparison of the Powell's formulation with Lighthill's formulation is shown in Fig. 7. The simulations using the integral form Lighthill's analogy for the current problem were presented in Ref. [11]. As mentioned earlier, the two formulations are mathematically equivalent, when the fluctuations in the kinetic energy are negligible. In Fig. 7, numerically some differences are observed broadband in the overall noise spectra of the two methods. Though, the main component of noise predicted at the BPF is identical for both formulations.

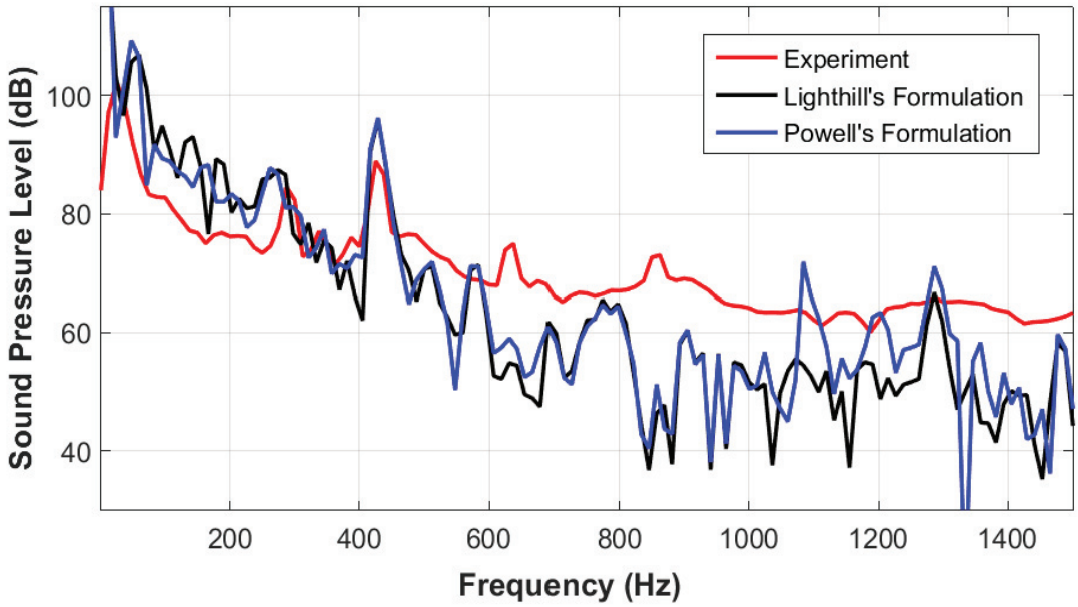


Figure 7 – Comparison of the sound pressure levels obtained using Powell's and Lighthill's formulations

### 4.4 A-weighted Sound Power Levels

In Fig. 8 the A-weighted sound power levels are presented using the 1/3rd Octave Band values. The BPF in the current problem falls into the band with the center frequency 400 Hz. An overall good agreement is observed up to 1400 Hz, when comparing the experimental and numerical results. Specifically, the peak values obtained at the 400 Hz center-frequency band are as follows: 79.61 dBA for the vortex sound based simulation, 79.13 dBA for the Helmholtz equation simulation, and 77.86 dBA for the measurement (red line). Moreover, the total sound power level summed over the first seventeen 1/3rd Octave bands (up to and including 2000 Hz center frequency) are 81.30 dBA, 80.38 dBA, and 79.45 dBA, respectively, for Powell's formulation, Helmholtz equation and the measurement.

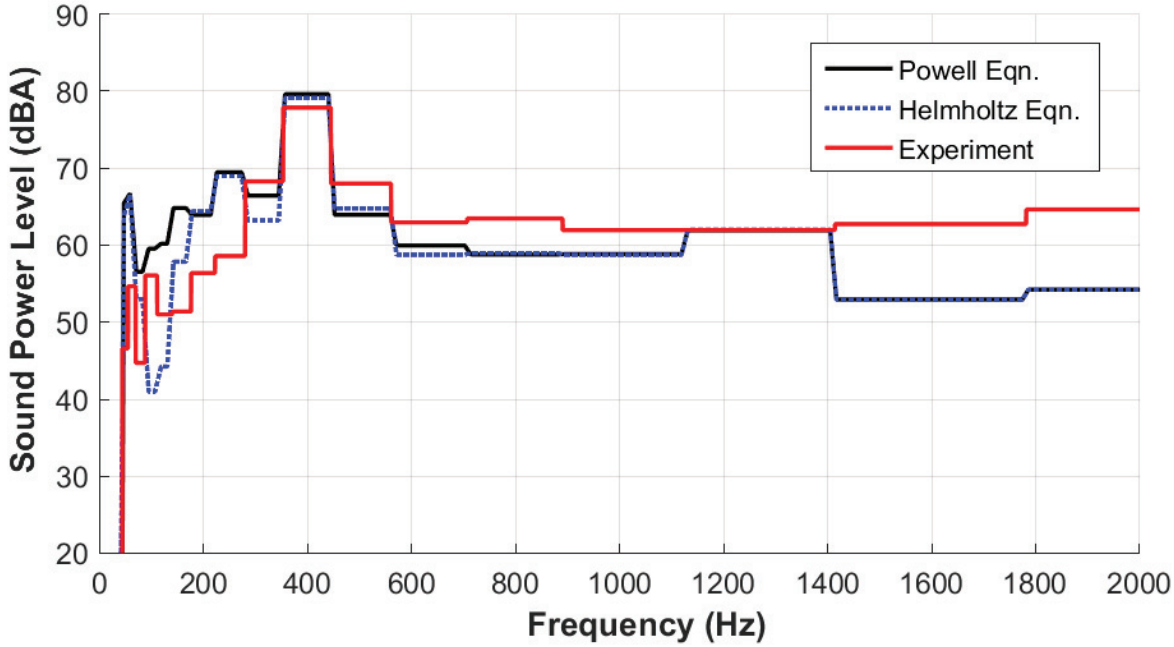


Figure 8 – A-weighted sound power levels obtained experimentally and numerically

We should finally note that there are two main correction factors in the interpretation of the measured noise values in the industrial norm ISO 5801. The first one is for the convective effects because of the flow velocity. For the current setup, this correction amounts to less than 0.2 dB for frequency values <1000 Hz. The second one is due to the turbulence screen protection of the microphones, and the corresponding values averaged over three microphones are given as a function of band center frequencies in Table 1. Clearly, the consideration of the turbulence screen protection as in Table 1 results in ~9 dB difference in the measured total sound power level. In the numerical simulations, such correction is not accounted for. Hence, the experimental spectrum in Fig. 8 has been plotted without taking into account the values in Table 1.

Table 1 – Measurement correction factor C2 for slit-tube screen of microphones

| Freq. (Hz) | 50 | 63 | 80 | 100 | 125 | 160 | 200 | 250 | 315 | 400 | 500 | 630 | 800 | 1000 |
|---|---|---|---|---|---|---|---|---|---|---|---|---|---|---|
| C2 (dB) | -1.77 | -4.3 | -2.3 | -2.10 | -1.24 | -0.65 | 0.18 | -2.19 | -2.48 | -3.07 | -3.44 | -3.01 | -3.47 | -3.28 |

## 5. CONCLUSIONS

In this study, the aeroacoustic noise of a centrifugal fan used in household dryers was investigated. The main objective of the current paper was the comparison of Lighthill's analogy and Powell's analogy for the low Mach number flow encountered in the application. The numerical simulations regarding such comparison have been performed using the integral forms of both formulations, where the main results are given in Figs. 7 and 8. It has been observed that the predicted sound pressure levels show minor differences. Handling of the numerical data, on the other hand, is considerably more convenient when using Powell's analogy, since the formulation involves vector variables (velocity and vorticity) instead of the tensor components. Good agreement between the experimental and the numerical sound power levels has been found. Further numerical studies will be performed for an aerodynamically optimized model of the radial fan, which was presented in Ref. [14].

## ACKNOWLEDGEMENTS

This work was funded by the German Ministry of Education and Research (Bundesministerium für Bildung und Forschung) within the research project High Efficiency Low Noise Heatpump Dryer (HELNOISE). The authors are thankful to the project partners ANSYS, B/S/H/ and GRONBACH for their support.



## REFERENCES

[1] C. Liu, Y. Cao, Y. Liu, W. Zhang, P. Ming. Numerical investigation of marine diesel engine turbocharger compressor tonal noise. *Proc. IMechE Part D: Journal of Automobile Engineering,* pp. 1-14, 2019.

[2] J. Prezelj, T. Novakovic. Centrifugal fan with inclined blades for vacuum cleaner motor. *Applied Acoustics,* Vol. 140, pp. 13-23, 2018.

[3] S. Lee, S. Heo, C. Cheong. Prediction and reduction of internal blade-passing frequency noise of the centrifugal fan in a refregirator. *International Journal of Refregiration,* Vol. 33, pp. 1129-1141, 2010.

[4] C. Eisenmenger, S. Frank, H. Dogan, M. Ochmann. Aerodynamische und aeroakustische Untersuchungen an Radialventilatoren mit rückwarts gekrümmten Schaufeln für Haushaltsgeräte, in *Deutsche Jahrestagung für Akustik (German Annual Conference on Acoustics) - DAGA*, Munich, 2018.

[5] Q. Datong, M. Yijun, L. Xiaolian, Y. Minjian. Experimental study on the noise reduction of an industrial forward-curved blades centrifugal fan. *Applied Acoustics,* Vol. 70, pp. 1041-1050, 2009.

[6] B. Jiang, J. Wang, X. Yang, W. Wang, Y. Ding. Tonal noise reduction by unevenly spaced blades in a forward-curved-blades centrifugal fan. *Applied Acoustics,* Vol. 146, pp. 172-183, 2019.

[7] W. Neise, G. H. Koopmann. Reduction of centrifugal fan noise by use of resonators. *Journal of Sound and Vibration ,* Vol. 73, Nr. 2, pp. 297-308, 1980.

[8] K. Paramasivam, S. Rajoo, A. Romagnoli. Suppression of tonal noise in a centrifugal fan using guide vanes. *Journal of Sound and Vibration,* Vol. 357, pp. 95-106, 2015.

[9] A. Powell. Theory of vortex sound. *Journal of Acoustic Society of America,* Vol. 36 (1), pp. 177-195, 1964.

[10] P. Martinez-Lera, A. Müller, C. Schram, P. Rambaud, W. Desmet, J. Anthoine. Robust aeroacoustic computations based on Curle's and Powell's analogies, in *Proceedings of ISMA*, 2018.

[11] H. Dogan, M. Ochmann, C. Eisenmenger, S. Frank. Prediction of the aeroacoustic noise of a radial fan using Ligthill's Analogy in frequency domain, in *Deutsche Jahrestagung für Akustik (German Annual Conference on Acoustics) - DAGA*, Rostock, 2019.

[12] C. Eisenmenger, S. Frank, H. Dogan, M. Ochmann. High Efficiency Low Noise Heatpump Dryer (HELNOISE), in *Deutsche Jahrestagung für Akustik (German Annual Conference on Acoustics) - DAGA*, Kiel, 2017.

[13] H. Dogan, M. Ochmann, C. Eisenmenger, S. Frank. A hybrid CFD/BEM method for the calculation of aeroacoustic noise from a radial fan, in *Deutsche Jahrestagung für Akustik (German Annual Conference on Acoustics) - DAGA*, Munich, 2018.

[14] C. Eisenmenger, S. Frank, H. Dogan, M. Ochmann. Aerodynamische und aeroakustische Optimierung eines Radialventilators mit rückwärts-gekrümmten Schaufeln für Haushaltsgeräte mittels Inverse Design, in *Deutsche Jahrestagung für Akustik (German Annual Conference on Acoustics) - DAGA*, Rostock, 2019.